CORPUS PUBLISHERS

Journal of Mineral and Material Science (JMMS)

ISSN: 2833-3616

Volume 6 Issue 4, 2025

Article Information

Received date : June 29, 2025

Published date: July 21, 2025

*Corresponding author

Gonzalo Blanco, Department of Geosciences, Eastern Regional University Center, University of the Republic, Route 8 km 282, Treinta y Tres, Uruguay

DOI: 10.54026/JMMS/1121

Key Words

Mineral; Iron; Metallurgy Industry; Quartz; Magnetite; Hydroxides

Research Article

SEM and EDS Mineral Analysis of the Cerro Papagayo Iron-Manganese Deposit from Uruguay

Gonzalo Blanco*, Ivan Tarjan, Paulina Abre, Camila Zunino and Daniel Segovia

Departamento de Geociencias, Centro Universitario Regional del Este, Universidad de la República, Ruta 8 km 282, Treinta y Tres, Uruguay

Abstract

The mineralogy of the Cerro Papagayo Fe-Mn deposit after beneficiation, involving crushing and magnetic separation is studied by SEM-EDS analysis. The ore and the mineral concentrate show a great mineral complexity with the presence of quartz, Mn-bearing silicate phases and Fe-Mn oxides of the magnetite-jacobsite series and high Mn oxides such as braunite, byxbite and hausmanite. The spessartine garnet and Mn-clinopyroxene are the most abundant silicates. Mn-Fe-Al hydroxides shows botroidal porous texture with high phosphorous content up to 1.5 wt% and identified as a probable contaminant for the Fe concentrate. The abundant presence of Mn-Fe oxides mineral grains up to 1 mm of the gangue mineral suggest their evaluation as a potential resource of Mn.

Introduction

Micro-XRF and particle image analysis using a scanning electronic microscope are fundamentals tools to evaluate the distribution and the possibility of liberation of the gangue and ore minerals during processing, [1-3]. The main objective of this work is the analyze the petrography and mineral chemistry of the procced Papagayo Iron deposit located in Uruguay. In order to accomplish the main objective, the studied material was selected from: 1) the raw Fe ore after crushing, 2) the Fe ore concentrate after crushing and magnetic separation and 3) the gangue minerals after crushing and magnetic separation. Secondly, chemical and textural analysis of the mineral species containing Mn is an important goal to evaluate the possibility to obtain a byproduct rich in Mn after the necessary modifications of the current separation process.

Mining and Geological Background

Pioneers since the 20th century recognized the presence of Fe and Mn occurrence in northern Uruguay and particularly in the Zapucay Area [4,5]. The presence of important reserves of Fe and Mn in Uruguay were recognized [6] and the "Instituto Uruguayo de Geología" and the USGS demonstrated Cerro Papagayo occurrence as exploration target [7]. The information of the Fe-Mn deposits in the Zapucay area including the Cerro Papagayo deposit was summarized including important geological information [8]. Recently some exploration companies positively evaluate the presence of iron in the area (Figure 1) and since 2020 the Cerro Papagayo deposit is exploited by Dialeca SA principally suppling material to the cement and metallurgy industry. In order to concentrate the iron ore, the company uses magnetic separators and crushers to obtain a final product with a grain size less than 3 mm and 60% of iron concentrate. The deposit is enriched in manganese up to 5% but since this element is a constituent of a wide range of silicates and oxidized minerals the beneficiation process is beyond the company´s consideration.

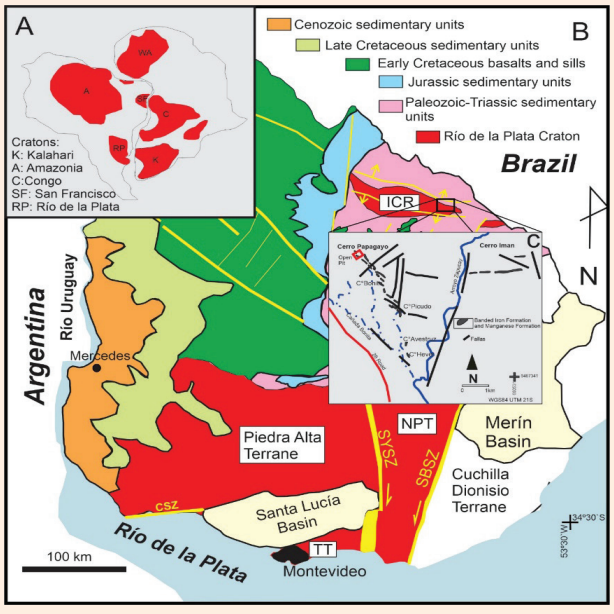

Figure 1: A: Location of The Río de la Plata Craton. B: Simplified and modified Uruguayan geological map [13], [15] ICR: Isla Cristalina de Rivera, SYSZ: Sarandí del Yi Shear Zone, SBSZ: Sierra Ballena Shear Zone, CSZ: Colonia Shear Zone, TT: Tandilia Terrane. C: Sketch map showing the distribution of the Iron Deposit in the Zapucay Area [8].

The Cerro Papagayo Iron deposit is located in the Precambrian Basement of Uruguay, so-called the Río de la Plata Craton, which comprises the Nico Pérez, Piedra Alta and Tandíl Terranes, with ages ranging from the Archean to the Neoproterozoic (Figure 1), [9]. The Isla Cristalina de Rivera is part of the Nico Pérez Terrane and is composed of metamorphosed gneisses and granulites displaying Paleoproterozoic ages between 2.2 and 2.05 Ga, and later intruded by ca. 580 Ma Neoproterozoic Granites [10]. The regional metamorphism and the hydrothermal metasomatism affected de mineral distribution and iron mineralization of the Papagayo deposit [11]. In particular, the magnetite recrystallization after the deposition and intense metamorphism of the Banded Iron Formations under granulitic conditions was the main event triggering the iron mineralization during the Paleoproterozoic on the Isla Cristalina de Rivera [11]. The BIFs are part of the Cerro Vichadero Formation [11] and correlate with other Paleoproterozoic BIF´s containing Fe-Mn ores as the Paleoproterozoic Hotazel Formation of the Transvaal Supergroup in the Kuruman Manganese Field [12]. The Vichadero Formation [11] is composed of: a) Banded Iron Formations (BIF), b) Manganese Formations (MnF), c) Quartzites, d) clinopyroxenites, e) calc-silicates, f) forsterite marbles and g) metabasites. Based on their mineralogy and textures, the BIFs of Vichadero Formation are subdividing in four groups [11]: I) banded rocks composed of 99% quartz and Fe-oxide-layers, (BIF) II) banded rocks composed of quartz, Fe and Mn oxides, clinopyroxene, amphiboles and subordinate garnets (BIF), III) garnet-rich rocks with Fe and Mn oxides, clinopyroxene and quartz (MnF/BIF), and IV) Mn-rich massive rocks, scarce quartz, Fe and Mn oxides, olivine, garnet, clinopyroxene and braunite (MnF/BIF).

Methodology

Three samples of 5 kg each were collected after the milling operation in the company plant. The sample IT01 consists of the Fe concentrate up to 60% and sample IT02 its representative of the gangue after the crushing and magnetic separation. Sample IT03 is the Fe ore after crushing. Grain size is less than 3 mm for the 3 samples. The samples were processed and analyzed in the Laboratorio de Geología del Departamento de Geociencias del Centro Universitario Regional del Este. Quartering apply to each sample and an aliquot were selected to fill 1 inch in diameter cup with the sample and epoxy. The obtained epoxy resin discs were polished using a diamond paste of 3 µm, 1 µm and 1/4 µm to obtain a mirror-like surface. Light microscopy analysis was carried out by Reflected Light Microscopy (RLM) which allowed identification of the main mineralogical phases and observation of some microstructural features [13,14]. Back-Scattered Electron imaging (BSE) and elemental analysis on the polished epoxy disc were done using a Jeol NeoScope JCM-6000 Plus equipped by an Energy-Dispersive X-Ray Spectrometry (EDS) consisting of one 10 mm^2 Silicon Drift Detector (SDD). 228 single-grain analysis of mayor and minor elements analysis were done according the recommendations [15]. Electrons are emitted by a traditional cartridge filament of W and hit the target at a distance of 19 mm. The X-ray take-off angle is about 25°. The energy resolution of the SDD is ~133 eV at the energy of Mn K_a (5894 eV). The EDS analyses were conducted using standard probe current (~30 nA), data collecting time of 60 s and accelerating voltage of 15 kv.

Results

The ore and gangue mineralogical composition show some similarities for the three samples as expected (Figure 2 and data repository). The iron concentrate (IT-01) is composed mainly of magnetite reaching up to 1.5 wt% Mn (Figure 3a and Table 1). The Mn oxides cross-cut the magnetite grains as veinlets between 5 and 10 µm in width and in some cases is composed of Braunite or Jacobsite-Magnetite. Nonmagnetic silicate and Mn-Fe oxide minerals are also common and are in grain contact or embedded within the magnetite (Figure 3a-3b). Pyroxene and spessartine garnets are well preserved with euhedral shapes and no compositional zoning. The gangue minerals (IT-02) show different characteristics than the previous samples as none of the single grain magnetic grains are preserved. Magnetite is usually trapped with quartz and other silicates and hematite also occurs. Noteworthy is the abundance of high Mn altered mineral grains with botryoidal texture forming irregular porous network composed of mineral aggregates of rhythmic alternation of oxides and hydroxides of Mn, Fe, and Al (Figure 4). These grains contain up to 1.5 wt% of P. Calcite grains are scarcely present. The Iron Ore (IT-03) is principally composed of quartz, magnetite, Mn-Fe oxides and silicates dominated by andradite garnet and subordinate Mn-pyroxene (Figure 5). The presence of altered hydroxide Mn-Fe-Al grains with botryoidal texture and the presence of some high P values up to 0.79 wt% is common. Mn-ilmenite was also detected though very scarce.

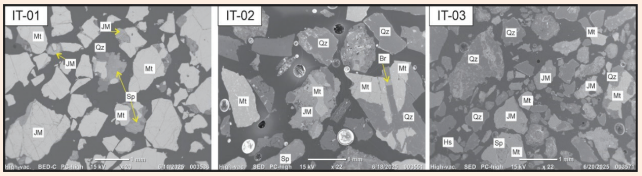

Figure 2: SEM-Backscatter images of the Fe concentrate (IT-01), the gangue (IT-02) and the Fe ore (IT-03).

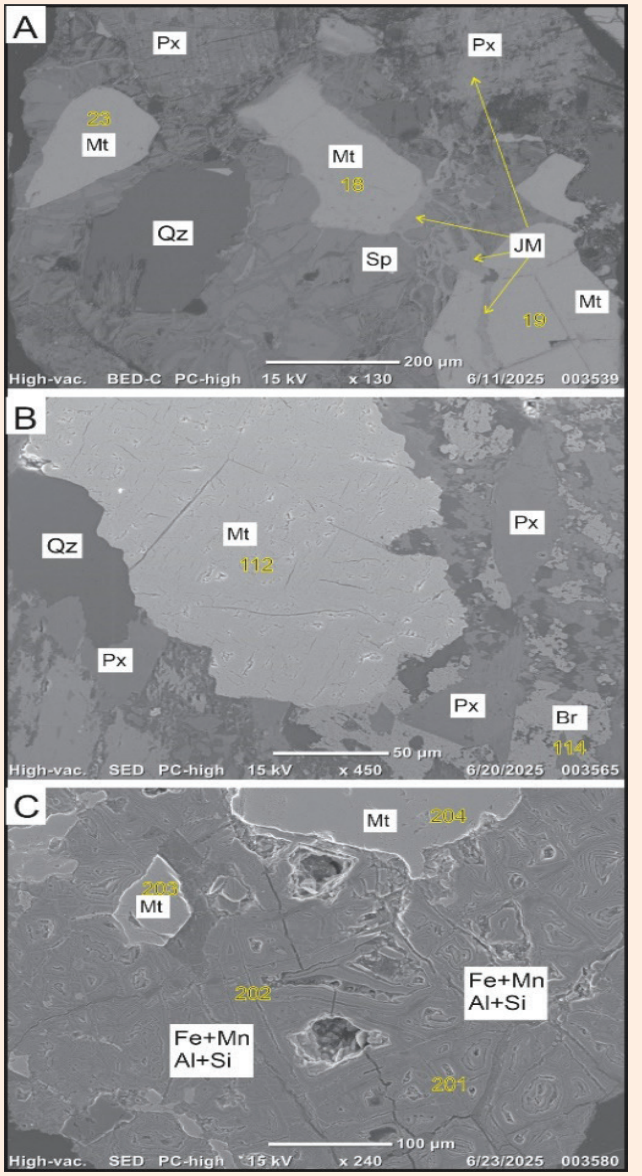

Figure 3: SEM-Backscatter images of A: composed grains of the Fe concentrate, note presence of spessartine (Sp) and pyroxene (Px) and veinlets of Mn oxide crosscutting the magnetite (IT-01) and B: gangue preserving some enclosed magnetite grains by silicates and Mn oxides (IT-02). B: Botruoidal and rhytmhic lamination of groutite MnO(OH), goethite FeO(OH) and diaspore AlO(OH) (IT-03).

Table 1: X-ray microanalysis (EDS) data from sample areas of Figures 3 and 5.

Point	FeO	MnO	Al_2O_3	SiO_2	P_2O_3	K_2O	Interpretation
18	97.4	0.8	0.4	0.5	0.0	0.1	Magnetite with silicates
19	97.5	1.3	0.5	0.3	ND	0.0	Magnetite with silicates
23	96.2	1.2	0.6	0.5	0.0	0.1	Magnetite with silicates
112	97.7	1.1	0.2	0.7	ND	0.0	Magnetite with silicates
114	1.7	88.0	0.2	9.1	0.1	0.2	Braunite with Pyroxene
201	37.6	28.8	17.9	12.6	0.7	0.2	Mn-Fe-Al Hydroxides
202	38.3	33.4	17.8	8.3	1.1	0.2	Mn-Fe-Al Hydroxides
203	97.9	0.5	0.3	0.5	0.1	0.1	Magnetite
204	98.8	0.6	0.1	0.3	0.1	0.0	Magnetite
208	23.2	68.3	1.2	1.2	0.4	3.3	Criptomelane and Braunite
209	11.5	76.8	1.3	1.3	0.3	6.1	Criptomelane and Braunite
210	47.0	21.8	5.2	21.8	0.3	1.4	Fe-Mn Pyroxene replacement
212	98.4	0.5	0.1	0.3	0.3	ND	Magnetite
85	2.3	94.9	0.5	1.7	0.1	0.4	Br-Hs with quartz
86	0.3	0.1	0.1	99.2	ND	ND	Quartz
87	97.6	0.7	0.4	0.6	0.1	0.0	Magnetite

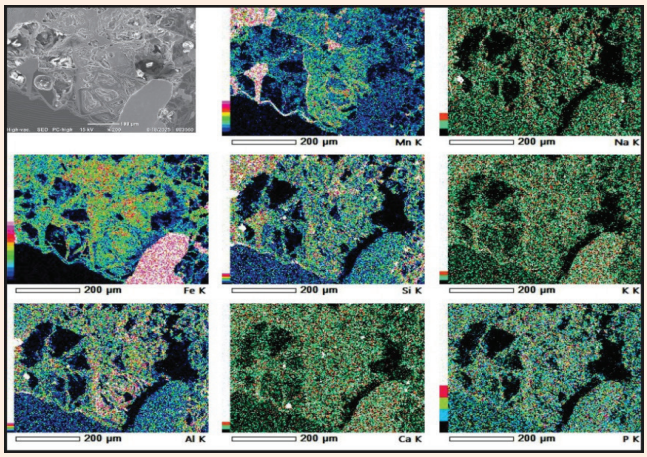

Figure 4: Compositional maps of a composed grain from the sample IT-02 showing the distribution of the Mn-Fe-Al hydroxides.

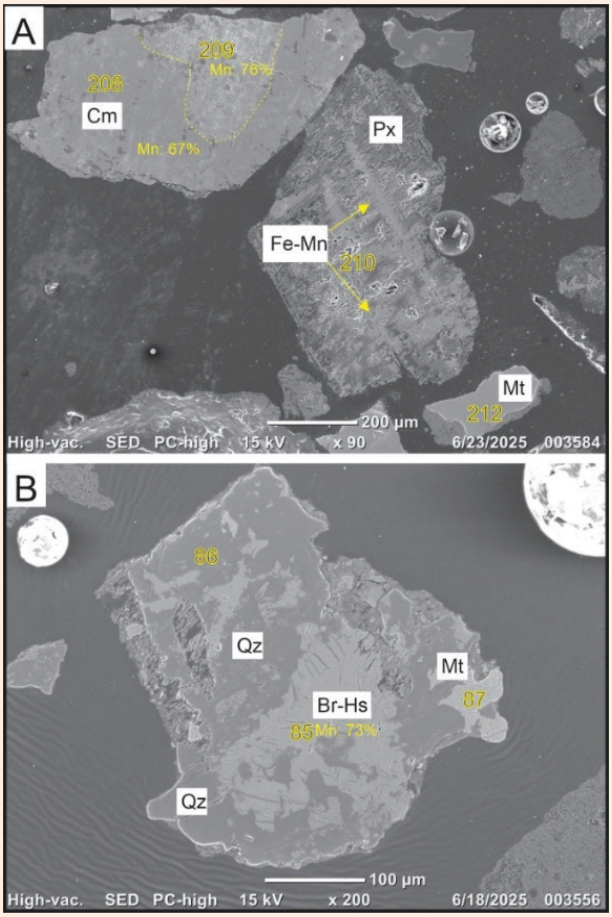

Figure 5: SEM-Backscatter images of the A: iron ore sample (IT-03) showing Fe-Mn oxides replacing piroxene and zoned criptomelane grain, and B: grain composed of braunita-hausmanite (Br-Hs), magnetite and quartz of the Fe concentrate sample (IT01).

Discussion and Conclusion

Textural and chemical analyses of the concentrate iron ore indicate that the magnetite is not the only mineral that contain Fe oxide. Waste minerals of the Fe-concentrate are composed by silicates and the Mn-Fe oxides and usually attached to the magnetite and actually not separable by magnetic procedures. P is a major contaminant in Fe Ore and usually is associated to Fe hydroxides like goethite [16]. In the ore concentrate, gangue and iron ore samples show the presence of hydroxides with botryoidal texture porous grains probably composed of an aggregate of groutite MnO(OH), goethite FeO(OH) and diaspore AlO(OH). The previous observation remarks the importance of considering the existence of this group of minerals for the beneficiation process, because the quality of the Fe concentrate could be improved after their separation [16]. The P shows a straight positive correlation with the Al content (Figure 6a) confirming petrographic observations related to Al hydroxides (Figure 4). In the Figure 6b the Mn vs Fe elements are plotted from the total of the Mn-Fe oxide minerals showing a negative correlation, suggesting that the solid solution series of Magnetite-Jacobsite are the main mineral component among the Mn ore, braunite, cryptomelane, byxbite and hausmanite are also detected and these minerals enrich the total Mn content of the ore [17]. Based on the petrographic and chemical analyses it is possible to distinguish two byproduct with differences in the Mn and P concentration, 1) Porous aggregate of groutite MnO(OH), goethite FeO(OH) and diaspore AlO(OH) minerals showing up to 1.5 wt% of P and 35 wt% average of Mn and, 2) Minerals of 0.1 to 1.0 mm in grain size composed of Fe-Mn oxides with average concentration of 0.08 wt% P and 54 wt% of Mn.

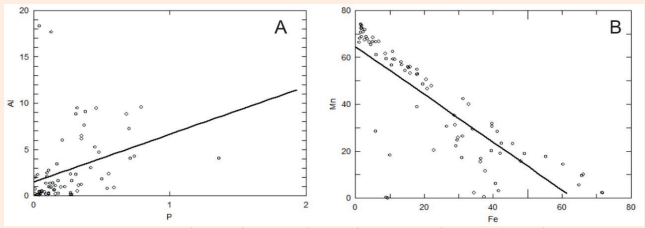

Figure 6: Diagram A shows the correlation between Al content vs the P content probably related to Mn-Fe-Al hydroxides composed grains of the 3 samples. B: indicate direct correlation between the Fe vs Mn of the minerals related to Jacobsite-Magnetite solid solution series. Some dispersion of the data indicate the analyzed high Mn oxides as grains and veinlets.

Acknowledgement

Dialeca SA for providing the material, the anonymous reviewer and the Editor are deeply acknowledged.

References

1. Santos LD, Brandao PRG (2003) Morphological varieties of goethite in iron ores from Minas Gerais, Brazil. Minerals Engineering 16(11): 1285-1289.
2. Santos LD, Brandao PRG (2005) LM,SEM and EDS study of microstructure of Brazilian iron ores microscopy and analysis. Analytical Science 19(1): 17-19.
3. Flude S, Haschke M, Storey M (2017) Application of benchtop micro-XRF to geological materials. Mineralogical Magazine 8(4): 923-948.
4. Kendall JD (1910) Report on the manganese ore deposits at Cerro Papagayo and Cerro Imán in Uruguay, South America. Friars House, New Broad Street, London EC, pp. 1-19.
5. Mastrander R (1916) Preliminary report on the mineral resources of the Eastern Republic of Uruguay. IGU Bulletin, No. 2, Uruguay.
6. Alvarado B (1962) Iron and manganese deposits in Uruguay. Report No. TAO/URU/4, United Nations.
7. Wallace RM (1962) Geological reconnaissance of some Uruguayan iron and manganese deposits in 1962. Open-File Report 76-466, Prepared in cooperation with Instituto Geologico del Uruguay and the United States Army Mission to Uruguay under the auspices of the Government of Uruguay and the Agency for International Development, U S Department of State By: Roberts Manning.
8. Bossi J, Navarro R (2000) Mineral resources of Uruguay. Montevideo, p. 416.
9. Bossi J, Cingolani C (2009) Extension and general evolution of the Río de la Plata Craton. In: Gaucher C, Sial AN, Halverson GP, Frimmel HE (Eds.), Neoproterozoic-Cambrian tectonics, global change and evolution: A focus on Southwestern Gondwana. Developments in Precambrian Geology, Elsevier, Netherlands, 16: 73-85.
10. Bossi J, Ferrando L (2001) Geological Map of Uruguay, version 2.0. Scale 1:500,000. Geoeditores. Montevideo, Uruguay.
11. Oyhantçabal P, Wagner-Eimer M, Wemmer K, Schulz B, Frei R, et al. (2012) Paleo- and Neoproterozoic magmatic and tectonometamorphic evolution of the Isla Cristalina de Rivera (Nico Pérez Terrane, Uruguay). International Journal of Earth Sciences 101: 1745-1762.
12. Ellis JH (1998) The Precambrian supracrustal rocks of the "Isla Cristalina de Rivera" in northern Uruguay and their ore deposits. Heidelberger Geowissenschaftliche Abhandlungen, Heidelberg, Germany, 90: 1-196.
13. Tsikos H, Moore JM (1997) Petrography and geochemistry of the Paleoproterozoic Hotazel iron formation, Kalahari Manganese Field, South Africa: Implications for Precambrian manganese metallogenesis. Economic Geology 92(1): 87-97.
14. Bossi J, Ferrando L (2001) Geological Map of Uruguay at a scale of 1/500,000, digital version 2.0. Faculty of Agronomy, Montevideo.
15. Blanco G, Abre P, Ferrizo H, Gaye M, Gamazo P, et al. (2021) Revealing weathering, diagenetic and provenance evolution using petrography and geochemistry: A case of study from the Cretaceous to Cenozoic sedimentary record of the SE Chaco- Paraná basin in Uruguay. Journal of South American Earth Sciences 105: 1-18.
16. Chen Y, Chen Yi, Liu Q, Liu Xi (2023) Quantifying common major and minor elements in minerals/rocks by economical desktop scanning electron microscopy/silicon drift detector energy-dispersive spectrometer (SEM/SDD-EDS). Solid Earth Sciences 8(1): 49-67.
17. Powncebya MI, Hapugodab S, Manuel J, Webstera NAS, MacRaea CM (2019) Characterisation phosphorus and other impurities in goethite-rich iron. Minerals Engineering 143: 106022.